Statistics of the Auger-Recombination of Electrons and Holes via Defect Levels in the Band Gap – Application to Lead-Halide Perovskites

Florian Staub[1], Uwe Rau[1] and Thomas Kirchartz[1,2*]
[1]IEK5-Photovoltaik, Forschungszentrum Jülich, 52425 Jülich, Germany
[2]Faculty of Engineering and CENIDE, University of Duisburg-Essen, Carl-Benz-Str. 199, 47057 Duisburg, Germany

ABSTRACT: Recent evidence for bimolecular non-radiative recombination in lead-halide perovskites poses the question for a mechanistic origin of such a recombination term. A possible mechanism is Auger recombination involving two free charge carriers and a trapped charge carrier. In order to study the influence of trap-assisted Auger recombination on bimolecular recombination in lead-halide perovskites, we combine estimates of the transition rates with a detailed-balance compatible approach of calculating the occupation statistics of defect levels using a similar approach as for the well-known Shockley-Read-Hall recombination statistics. We find that the kinetics resulting from trap-assisted Auger-recombination encompasses three different regimes: low-injection, high-injection, and saturation. While the saturation regime with a recombination rate proportional to the square of free carrier concentration might explain non-radiative bimolecular recombination in general, we show that the necessary trap density is higher than reported. Thus, we conclude that Auger recombination via traps is most likely not the explanation for the observed non-radiative bimolecular recombination in $CH_3NH_3PbI_3$ and related materials.

INTRODUCTION

One of the key prerequisites for optoelectronic materials are long non-radiative lifetimes[1-7] for recombination via defects as compared to the recombination coefficients for direct radiative band-to-band transitions.[8-13] Recombination via defects[14,15] is usually assumed to be mediated by the emission of multiple phonons[16-21] while band-to-band recombination via multiphonon emission is thought to be extremely unlikely in inorganic semiconductors.[22] Because the transition rates are strongly reduced for increasing number of phonons[17,22] involved in a single transition at low to moderate strength of electron-phonon coupling, direct band-to-band recombination is typically assumed to be entirely radiative in inorganic semiconductors. This is different in organic semiconductors due to the higher energy associated with molecular vibrations in organic molecules relative to the energy of phonons in inorganic semiconductors.[23] Given that lead-halide perovskites due to the high atomic mass of Pb and I have particularly low phonon energies,[24,25] it is initially rather surprising that there is evidence[26,27] for recombination terms that are quadratic in charge-carrier density (like radiative recombination in high level injection) and are non-radiative. In addition to multiphonon recombination, Auger recombination is the second archetypical non-radiative recombination mechanism.[13,28-30] Auger recombination involving two free electrons and one hole or two free holes and one electron, respectively, should be cubic in charge-carrier density in high level injection and would therefore not be able to explain the observed features. However, Auger recombination involving trapped charge carriers could in principle explain the observed quadratic behavior.[26]

Thus far, trap-assisted Auger recombination has been mainly discussed for the case of highly doped semiconductors[29-31] where this mechanism is most efficient because of the high density of free charge carriers. This implies that only the limiting linear case of low-injection (with respect to the doping level) is usually considered. In addition, it has been discussed in the context of determining limiting efficiencies for Si solar cells but recently also for perovskite solar cells.[13,28,30,32] In order to study the potential effect of trap-assisted Auger recombination on bimolecular recombination in lead-halide perovskites close to the radiative limit, a model for the full recombination statistics is required. Therefore, we develop a detailed balance compatible rate equation model in analogy to the Shockley-Read-Hall recombination statistics.[14,15] Subsequently, we use known material properties of lead-halide perovskites and previously derived equations[33] for the transition rates to estimate the Auger coefficients for trap-assisted Auger recombination in perovskites. Finally, we derive the necessary trap density for trap-assisted Auger recombination to explain the observed non-radiative contribution to bimolecular recombination. The necessary defect density is at least on the order of 10^{17} cm^{-3} for midgap defects and increases for more shallow defects. This defect density is about one order of magnitude higher than the defect densities that have so far been observed in experiment.[34,35] Thus, we conclude that trap-assisted Auger recombination is unlikely to be the reason for the observed non-radiative bimolecular recombination and probably does not pose a fundamental limitation to the efficiency of lead-halide perovskites.

RESULTS AND DISCUSSION

Recombination Statistics. The complete picture of Auger processes involving traps as outlined in Ref. [33] is illustrated in Fig. 1. In total four processes can be summarized by four transition coefficients $T_1 ... T_4$:

(1) two electrons e and an empty trap h_t transform into an electron e^* (at non-thermal energy) and a trapped electron e_t according to the reaction scheme: $2e + h_t \longleftrightarrow e^* + e_t$.

(2) an electron, a hole h, and an empty trap transform into a hole $h*$ (at non-thermal energy) and a trapped electron: $e + h + h_t \longleftrightarrow h * + e_t$.

(3) an electron, a hole, and a trapped electron transform into an electron (at non-thermal energy) and an empty trap: $e + h + e_t \longleftrightarrow e * + h_t$

(4) two holes and a trapped electron transform into a hole (at non-thermal energy) and an empty trap: $2h + e_t \longleftrightarrow h * + h_t$.

Thus, processes 1 and 2 result in electron capture and processes 3 and 4 are hole capture processes such that a net recombination of an electron-hole pair requires a combination of steps 1 or 2 with 3 or 4.

In order to fulfill the requirements of detailed balance, we also have to consider the back reactions, i.e. impact ionization of trapped electrons or holes via hot electrons or holes. The rates $R_{1..4,b}$ for the back reactions are determined by the Auger coefficients $C^*_{1..4}$ such that we have, e.g., for back reaction 1 $R_{1,b} = C^*_1 n * N$ where $n*$ denotes the concentration of hot electrons and N the concentration of filled traps. If we assume that the thermalization of charge carriers is faster than the Auger processes or their inverses, the ratio between $n*$ and the overall concentration n of electrons is constant and corresponds to the ratio n^*_0 / n_0 between both concentrations at thermal equilibrium. Thus, we define the coefficient $C_1 = C^*_1 n^*_0 / n_0$ and, analogously, $C_2 = C^*_2 p^*_0 / p_0$, $C_3 = C^*_3 n^*_0 / n_0$, and $C_4 = C^*_4 p^*_0 / p_0$ using p^*_0, p_0, $p*$, and p as the analogous variables for holes. Then, the rates for the four transitions can be written as

$$R_1 = T_1 n^2 (N_T - N) - C_1 nN = T_1 \left[n^2 (N_T - N) - nn_1 N \right], \tag{1}$$

$$R_2 = T_2 np(N_T - N) - C_2 pN = T_2 \left[np(N_T - N) - pn_1 N \right], \tag{2}$$

$$R_3 = T_3 npN - C_3 n\left(N_T - N\right) = T_3\left[npN - np_1\left(N_T - N\right)\right], \tag{3}$$

and

$$R_4 = T_4 p^2 N - C_4 p\left(N_T - N\right) = T_4\left[p^2 N - pp_1\left(N_T - N\right)\right]. \tag{4}$$

Here, we use the abbreviations

$$n_1 = N_C \exp\left(\frac{E_C - E_T}{kT}\right) = n_0 \frac{N_T - N_0}{N_0} \tag{5}$$

and

$$p_1 = N_V \exp\left(\frac{E_T - E_V}{kT}\right) = p_0 \frac{N_0}{N_T - N_0}, \tag{6}$$

where n_0 and p_0 are the equilibrium concentrations of electrons and holes. The concentrations n_1 and p_1 correspond to the values of n and p, when the Fermi level lies at the trap depth E_T. We eliminate the parameters $C_1, \ldots C_4$ in Eqs. (1) to (4) by using the principle of detailed balance[36] and expressing them as a product of $T_1, \ldots T_4$ multiplied with either n_1 or p_1 in analogy to the derivation of Shockley-Read-Hall statistics. By assuming steady-state conditions $dN/dt = 0$, we may eliminate the concentration N of filled traps by writing

$$R_1 + R_2 = R_3 + R_4 . \tag{7}$$

We then obtain for the (normalized) density of occupied trap states

$$\frac{N}{N_\mathrm{T}} = \frac{T_1 n^2 + T_2 np + T_3 np_1 + T_4 pp_1}{T_1\left(n^2 + nn_1\right) + T_2\left(np + pn_1\right) + T_3\left(np + np_1\right) + T_4\left(p^2 + pp_1\right)} . \tag{8}$$

The final recombination rate R_TA is subsequently given by inserting Eq. (8) into $R_\mathrm{TA} = R_1 + R_2 = R_3 + R_4$ and is given by

$$\frac{R_\mathrm{TA}}{N_\mathrm{T}} = \frac{\left(np - n_1 p_1\right)\left(T_3 n + T_4 p\right)\left(T_1 n + T_2 p\right)}{T_1\left(n^2 + nn_1\right) + T_2\left(np + pn_1\right) + T_3\left(np + np_1\right) + T_4\left(p^2 + pp_1\right)} . \tag{9}$$

Simulation Results. Figure 2a illustrates Eq. (9) as a function of the excess-charge carrier concentration $\Delta n = n - n_0$ using the parameters given in table 1. The rate of Auger recombination involving interactions with defect states exhibits three regimes with different dependencies of R_{TA} on the excess-charge carrier concentration Δn. We assume the semiconductor to be p-type ($n_0 << p_0$) in this example (doping density $N_{\mathrm{A}} = 3 \times 10^{15}$ cm^{-3})[37], thus, for $\Delta n << N_{\mathrm{A}}$, we are in low-level injection conditions. In addition, we assume the defect to be close to the conduction band, i.e. $n_1 >> p >> p_1$. In this case, Eq. (9) simplifies to

$$\frac{R_{\mathrm{TA}}^{\mathrm{low}}}{N_{\mathrm{T}}} = \frac{T_4 N_{\mathrm{A}}^2}{n_1} n\,, \tag{10}$$

i.e. the recombination rate scales linearly with $\Delta n = n$. This linear scaling is independent of the position of the trap and would also happen for a midgap trap, in which case, the rate would be

$$\frac{R_{\mathrm{TA}}^{\mathrm{low}}}{N_{\mathrm{T}}} = T_2 N_A n\,. \tag{11}$$

For higher excess charge densities, $\Delta n > N_{\mathrm{A}}$, we enter high-level injection conditions, where we may simplify Eq. (9) using the conditions $n_1 >> n = p = \Delta n >> p_1$ (for a trap close to the conduction band edge). Then, we obtain

$$\frac{R_{\mathrm{TA}}^{\mathrm{high}}}{N_{\mathrm{T}}} = \frac{T_3 + T_4}{n_1} n^3 \tag{12}$$

i.e. a cubic relation between the rate and the excess carrier concentration. Only in the saturation regime, where $n = p = \Delta n >> n_1 >> p_1$, the recombination rate

$$\frac{R_{\mathrm{TA}}^{\mathrm{sat}}}{N_{\mathrm{T}}} = \frac{(T_1 + T_2)(T_3 + T_4)}{T_1 + T_2 + T_3 + T_4} n^2 \tag{13}$$

starts to scale quadratically with Δn. Thus, the three regimes visible in Figure 2a differ from the situation encountered for Auger recombination of free charge carriers. Here, also three regimes are visible, but the order for the Auger recombination rate R_{A} (for free carriers) is $R_{\mathrm{A}} \sim \Delta n$ (for low level injection), $R_{\mathrm{A}} \sim \Delta n^2$ (for $n \approx p$) and $R_{\mathrm{A}} \sim \Delta n^3$ for high level injection. In contrast Auger recombination via traps features an intermediate cubic scaling law as long as the doping concentration is smaller than either n_1 or p_1. In order to estimate the magnitude of trap-assisted Auger recombination for the specific case of lead-halide perovskites, we use equations for the transition coefficients $T_1, \ldots T_4$ derived by Landsberg et al.[33] which are given by

$$T_i = \frac{8q^4\mathrm{h}^3}{\left(m_{\mathrm{eff}}\varepsilon_0\varepsilon_{\mathrm{r}}\right)^2} N_i \left[1 + \frac{d_{i1}}{b_i} + \frac{d_{i2}}{4b_i^2}\right], \tag{14}$$

where table 2 provides the values for the abbreviations N_i, d_i and b_i for $i = 1\ldots 4$.

Figure 2b shows the resulting effective lifetime τ_{eff} for trap assisted Auger recombination assuming a high trap density of 10^{18} cm^{-3}. We define the effective lifetime for a given process as $\tau_{\mathrm{eff}} = \Delta n/R$, where R is the recombination rate for a certain recombination mechanism. The effective lifetime τ_{TA} for trap assisted Auger recombination is therefore defined as $\tau_{\mathrm{TA}} = \Delta n/R_{\mathrm{TA}}$, while the effective radiative lifetime is $\tau_{\mathrm{rad}} = \Delta n/R_{\mathrm{rad}}$. Here R_{rad} is the radiative recombination rate. We note that for low excess charge carrier concentrations Δn, both the trap-assisted Auger recombination and radiative recombination lead to a constant effective lifetime, consistent with the recombination rate increasing linearly with Δn in both cases. Once Δn exceeds the doping concentration assumed to be $N_{\mathrm{A}} = 3 \times 10^{15}$ cm^{-3}, the Auger lifetime is dropping drastically until $\Delta n \approx n_1$, at which point the slope gets flatter again. This is the logical consequence of the three regimes for R_{TA} seen in Fig. 2a. We also note that even for such a high trap density of $N_{\mathrm{T}} = 10^{18}$ cm^{-3}, the radiative lifetime is lower for all values of Δn.

Figures 2c and d show the situation of a deep trap first for the recombination rate (c) and subsequently for the effective lifetime (d). For deep traps, n_1 is very small ($n_1 << N_{\mathrm{A}}$), thus there exist only two regimes (low injection and high injection) but no saturation regime. In consequence, the effective lifetimes for radiative and trap-assisted Auger recombination have the same shape. For the assumed values of k_{rad} and N_{T}, the values for τ_{TA} and τ_{rad} are quite similar. In figure 2d, we also show for comparison the effective Shockley-Read-Hall lifetime via a deep trap. We do these calculations based on the theory of multiphonon recombination discussed in ref. [22] and based on refs. [17] and [18]. Here, we observe that for trap densities already much lower than used for Auger recombination via traps, the SRH lifetime dominates over a wide range of Δn values.

Having established the general features of the recombination statistics of Auger recombination involving traps, we now want to investigate more closely under which circumstances the recombination rate is comparable to the radiative recombination rate. In particular, we are interested in the case described by Eq. (13), where the scaling is quadratic. In this scenario, we may define the total bimolecular recombination rate R_{bm} as

$$\begin{aligned} R_{\mathrm{bm}} &= k_{\mathrm{eff}} n^2 = k_{\mathrm{rad}} n^2 (1 - p_{\mathrm{r}}) + R_{\mathrm{TA}}^{\mathrm{sat}} \\ &= \left[k_{\mathrm{rad}} (1 - p_{\mathrm{r}}) + \frac{(T_1 + T_2)(T_3 + T_4)}{T_1 + T_2 + T_3 + T_4} N_{\mathrm{T}} \right] n^2 \ , \\ &= \left[k_{\mathrm{rad}} (1 - p_{\mathrm{r}}) + k_{\mathrm{TA}} (N_{\mathrm{T}}) \right] n^2 \end{aligned} \tag{15}$$

i.e. the sum of radiative recombination ($k_{\mathrm{rad}} n^2$), minus the amount of light that is reabsorbed and contributes to internal generation ($p_{\mathrm{r}} k_{\mathrm{rad}} n^2$, with p_{r} being the probability of reabsorption[37,38]) plus the trap-assisted Auger recombination. Figure 3 (a) illustrates the effective Auger coefficient $C_{\mathrm{T}} \equiv k_{\mathrm{TA}}/N_{\mathrm{T}}$ as a function of trap depth E_{T}. As it is the case for Shockley-Read-Hall statistics, also the Auger recombination rate via defects shows its maximum for mid-gap traps, when detrapping of captured charge carries is least likely. The vertical dashed lines represent intrinsic defect levels according to density functional theory calculations as reported in ref. [39]. In the next step, we evaluate the defect density N_{T}, which has to be present in the samples in order to cause a certain non-radiative bimolecular recombination coefficient k_{non}. Table 3 shows experimental data from various groups on the total, radiative and non-radiative bimolecular recombination coefficient. The values for the non-radiative recombination coefficient vary quite strongly. Therefore, we vary k_{non} in the range between 10^{-12} to 10^{-10} cm^3/s and show the necessary trap density as a function of trap position in Fig. 3b. In comparison, we show the necessary trap depth to achieve a monomolecular Shockley-Read-Hall type lifetime $\tau_{SRH} = 1$ µs assuming multiphonon transitions as discussed in ref. [22]. We judge from Fig. 3b that deep trap densities > 10^{17} cm^{-3} are needed for midgap traps and higher for shallower traps. While such trap densities at midgap would lead to very short SRH lifetimes that are not consistent with experiment, such trap densities may explain experimental data if the trap is not midgap but at a trap depth of around 0.5 to 0.6 eV away from either the conduction or valence band. In order to put these densities into context, table 4 compares trap densities that have been measured on $CH_3NH_3PbI_3$ in the literature. Table 4 suggests that so far most experimentally observed trap densities are in the range of 10^{15} to 10^{16} cm^{-3}, i.e. in a range that would not lead to substantial trap assisted Auger recombination.

Discussion and Outlook. Having established that Auger recombination via traps is not likely to explain the observed non-radiative contributions to bimolecular recombination, it is useful to discuss the implications of this result and consider alternative explanations for the observed trends. First, we want to state that most experimental approaches to study bimolecular recombination would not be sensitive to whether bimolecular recombination is radiative or non-radiative. In most cases, the transient decay is fitted with a model that accounts for bimolecular recombination. In case of transient photoluminescence experiments it is clear that some of this recombination has to be radiative in order to generate a signal but the determination of how much of this bimolecular recombination is radiative would require additional information. This additional information can either be another experiment that determines total recombination as done by Richter et al[26] or some experimental circumstances that would distinguish radiative from non-radiative such as the sensitivity of radiative recombination to parasitic absorption via the modulation of the photon recycling probability as done previously by us.[27] Certainly two sets of experimental evidence, we are aware of, are not very much and future will tell whether these results are reproduced by others or are a peculiar feature of the samples or the data analysis in these papers. However, assuming that the data is representative, we want to briefly explore what other explanations there might be.

In a simple zero-dimensional picture, the authors are not aware of any recombination mechanism that would be quadratic in charge-carrier density and still non-radiative other than the one discussed here. Thus, it is logical to explore effects requiring more dimensions. There are essentially two options in our opinion: (i) Diffusion of carriers at high level injection inside the films leads to a decrease in signal that could be interpreted as recombination but isn't or (ii) lateral inhomogeneous lifetimes lead to a distribution of decay times that creates a decay that appears quadratic in charge carrier density but is not related to locally quadratic recombination mechanisms. Let us briefly look into the two options in more detail. After excitation of a sample with a laser pulse electrons and holes are created based on the generation profile of the sample. Disregarding interferences it is clear that more electrons and holes would be created close to the front surface of the sample and less towards the back. As long as electron and hole concentrations are roughly equal, the luminescence is higher than after equilibration of the charge carrier distribution. This leads to a decay in the luminescence that requires no recombination to happen. Diffusion of charge carriers during a transient photoluminescence experiment has been taken into account in the classical theory papers on transient PL experiments,[40,41] in first experiments on perovskite films with contact layers[42] and in the case of transient experiments on perovskite crystals.[43,44] However, given the range of mobilities that is commonly reported,[45,46] diffusion and equilibration of charge carriers in a film of few hundreds of nm thickness should happen in the sub-ns range (e.g. ~ 300 ps for a 300 nm film and a mobility of 20 $\mathrm{cm^2/Vs}$). Thus, in order for this explanation to affect the experiments there have to be at least some charge carriers with a substantially lower mobility in order to see an effect on the time scale where bimolecular recombination is typically observed.

The second option is laterally inhomogeneous lifetimes that have been reported and studied in a range of publications.[47,48] If by averaging over a certain area, the macroscopic decay curve does not capture one lifetime but a broad distribution of lifetimes, the tail of this distribution towards shorter lifetimes could influence the shorter time scales of a transient photoluminescence experiment and thereby affect the way we interpret the data. Future work of modelling the photoluminescence in two or three dimensions will have to show whether this is a likely explanation for the observed data in references [26,27]. Both of these alternative approaches to explain the experimental data would not be a unique feature of every MAPI sample but instead could vary from sample to sample. They would therefore not contradict reports[6,7] of extremely high photoluminescence quantum efficiencies that leave little room for additional non-radiative pathways.

CONCLUSIONS

In summary, we have developed a rate model for the full recombination statistic of electrons and holes via trap-assisted Auger recombination. The model covers the linear low-injection case with a recombination rate $R_{\mathrm{TA}} \propto \Delta n$ proportional to the density of excess charge carriers Δn, as well as two non-linear situations, namely high-level injection with $R_{\mathrm{TA}} \propto \Delta n^3$ and the saturation situation with $R_{\mathrm{TA}} \propto \Delta n^2$. The latter case represents the bi-molecular recombination that directly competes with radiative recombination. As an example, our calculations following the theory of Ref.[33] yield the actual rates for the case of $CH_3NH_3PbI_3$. The coefficients for this specific case are however relatively small. Therefore, we conclude that this mechanism is not likely to be the origin of experimentally measured non-radiative bimolecular recombination coefficients.

AUTHOR INFORMATION

Email: t.kirchartz@fz-juelich.de (corresponding author)

Email: u.rau@fz-juelich.de

Email: f.staub@fz-juelich.de

Notes

The authors declare no competing financial interest.

ACKNOWLEDGEMENTS

TK and UR acknowledge support from the DFG (Grant Nos. KI-1571/2-1 and RA 473/7-1) and from the Helmholtz Association via the PEROSEED project. TK thanks Igal Levine (Weizmann, Rehovot) for sharing most of the references for table 4.

Table 1: Input parameters used for the calculations presented in Figures 2 and 3 if not otherwise stated. There are various reported values for the effective mass of electrons and holes in the literature that are ranging from ~0.1 to ~0.3.[37,49-53] Here we use a value of $0.2m_0$ for simplicity where m_0 is the electron rest mass.

band gap	E_g	1.6 eV
effective mass of electrons	m_e	$0.2m_0$
effective mass of holes	m_h	$0.2m_0$
relative permittivity	ε_r	33.5 [24]

Table 2: Definition of the abbreviations used to determine the trap assisted Auger recombination coefficients T_i using Eq. (15). Here, E_g is the band gap, E_t is the trap depth with respect to the conduction band, $\sigma = m_\mathrm{h}/m_\mathrm{e}$ is the ratio of the hole and electron effective mass and $\sigma_\mathrm{L} = 1/\sigma$. In this form, the notation is valid for free electrons in the conduction band interacting with defect states. For free holes in the valence band, E_t, σ and σ_L have to be adjusted accordingly.

i	***N_i***	***d_{i1}***	***d_{i2}***	***b_i***
1	$\frac{1}{16E_t^3}$	13	-260	$\frac{2E_t}{kT}$
2	$\frac{\sigma_L^{9/2}}{(1+\sigma_L)^4 E_t^3}$	$0.5(33-15\sigma_L)$	$0.5(33-15\sigma_L)$	$\frac{(1+\sigma_\mathrm{L})E_t}{kT}$
3	$\frac{E_t^{5/2}}{(E_g-E_t)^{3/2}E_g^4}$	$-2-6\sigma+\left(1-\frac{E_t}{E_g}\right)$ $\times\left(20(1+\sigma)-\frac{3}{2}\right)$	$30(1+\sigma)(5\sigma-3)+\frac{15}{\left(1-\frac{E_t}{E_g}\right)^2}$ $-1200\left(1-\frac{E_t}{E_g}\right)(1+\sigma)^2$ $+1680\left(1-\frac{E_t}{E_g}\right)^2+\frac{24(1+3\sigma)}{\left(1-\frac{E_t}{E_g}\right)}$	$\frac{E_g}{kT}$
4	$\frac{\sigma_L^{9/2}E_t^{5/2}}{(E_g-E_t)^{3/2}(\sigma_L E_t+E_g-E_t)^4}$	$-8-40.5$ $\times\frac{E_g-E_t}{E_g-(1+\sigma_L)E_t}$	$40(11+120w+168w^2)$ $+\frac{64}{w}-\frac{27}{w^2}$ $w=\frac{E_g-E_t}{E_g-(1+\sigma_L)E_t}$	$\frac{E_\mathrm{g}-(1-\sigma_\mathrm{L})E_t}{kT}$

Table 3: Values for the bimolecular recombination coefficients in units of cm^3/s of $CH_3NH_3PbI_3$ from literature. Notes: (a) Data from ref. [37] corrected using the evidence from ref. [27] that only 66% of the bimolecular recombination is radiative. (b) Measurements done at different thicknesses. (c) Samples with PbI_2 precursor and (d) samples made from $PbCl_2$ precursor.

Reference	k_{ext} **(cm^3/s)**	k_{rad} **(cm^3/s)**	k_{non} **(cm^3/s)**
Staub et al.[37]	4.78×10^{-11}	8.7×10^{-10}	neglected
Staub et al.[27,37a]	4.78×10^{-11}	8.4×10^{-11}	4.4×10^{-11}
Crothers et al.[54b]	1.4×10^{-10} to 2×10^{-11}	6.8×10^{-10}	0
Richter et al.[26c]	8.1×10^{-11}	7.1×10^{-11}	7.2×10^{-11}
Richter et al.[26d]	7.9×10^{-11}	1.8×10^{-10}	5.6×10^{-11}

Table 4: Trap densities reported for $CH_3NH_3PbI_3$ thin films in the literature.

Reference	**Method**	**trap density (cm^{-3})**	**trap depth E_T (eV)**
Baumann et al.[34]	thermally stimulated current (TSC)	$>10^{15}$	~ 0.5
Landi et al.[55]	noise spectroscopy	4×10^{15}	~ 0.8
Heo et al.[56]	deep level transient spectroscopy (DLTS)	$\sim 10^{15}$	0.62
		$\sim 10^{15}$	0.75
Levine et al.[57]	steady state photocarrier grating	$>10^{16}$	recombination center
Gordillo et al.[58]	TSC	9×10^{16}	0.18
		5×10^{16}	0.49
Duan et al.[59]	Admittance Spectroscopy	$\sim 10^{16}$ cm^{-3}	0.16
Heo et al.[60]	Admittance Spectroscopy	$\sim 10^{16}$ cm^{-3}[a]	0.27
		$\sim 10^{17}$ cm^{-3}[b]	0.28
Yang et al.[35]	DLTS	9×10^{13} to 5×10^{14} cm^{-3}	0.78

---

[a] DMF as solvent with HI as additive

[b] DMSO as solvent

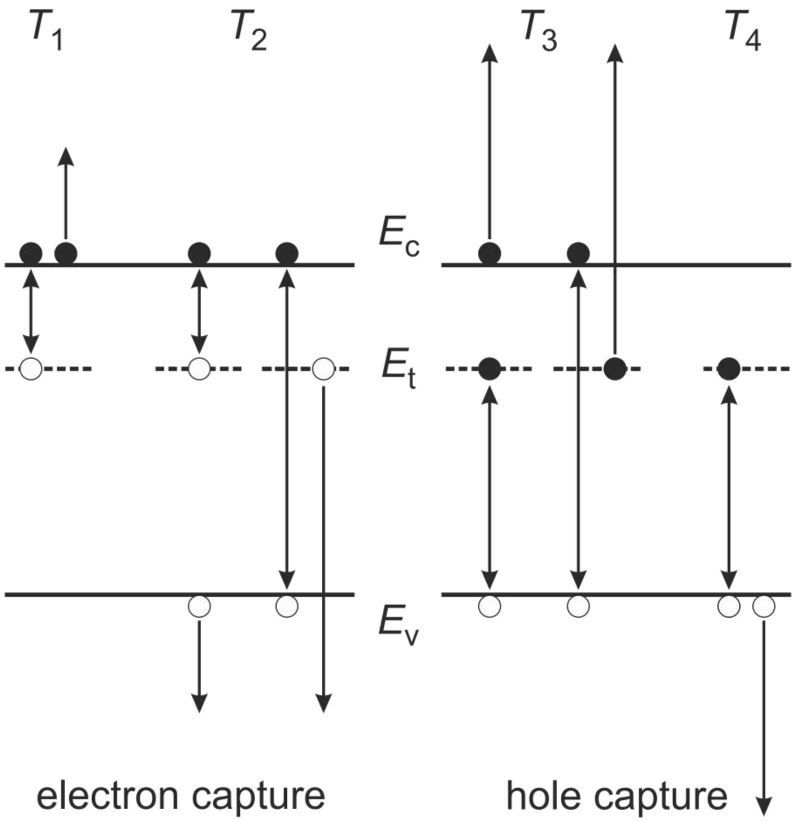

Figure 1: Illustration of various interactions between free charge carriers and defect states resulting in electron capture (with coefficients T_1, T_2) and hole capture (T_3, T_4), respectively. Please note that the processes 2 and 3 consist two possible interactions each. The energy levels of the valence and conduction band are here denoted as E_V and E_C, respectively. Furthermore, E_t marks the imperfection level (trap depth).

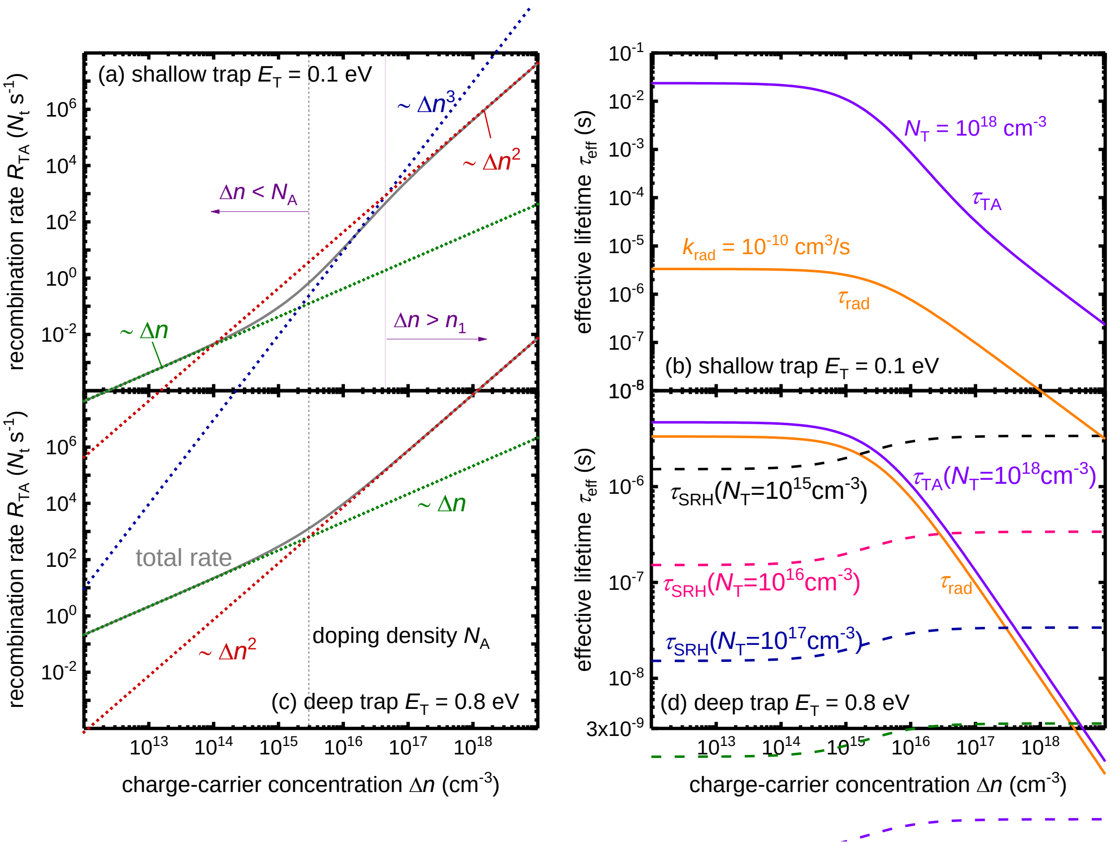

Figure 2: (a, b) Recombination rate and (c,d) effective lifetime as a function of charge-carrier concentration. (a) shows the situation of a shallow trap (E_T = 0.1 eV) with the solid grey line indicating the total trap assisted Auger recombination and the dotted lines illustrate the approximations given by eqs. (10), (12) and (13) valid in three different injection regimes. (b) shows the equivalent plot for the case of a midgap trap which only shows a linear regime at low Δn and a quadratic regime at high Δn. (c) shows the effective lifetime τ_{eff} for Auger recombination via traps assuming a trap density N_T = 10^{18} cm^{-3} and the radiative lifetime τ_{rad} = $\Delta n/R_{rad}$ assuming $R_{rad} = k_{rad}np$ with k_{rad} = 10^{-10} cm^3/s. (d) shows the effective lifetime for a deep trap. For comparison, we also added the values for SRH recombination using capture coefficients determined as discussed in ref. [22] and using different trap densities that are lower than the one for trap assisted Auger recombination.

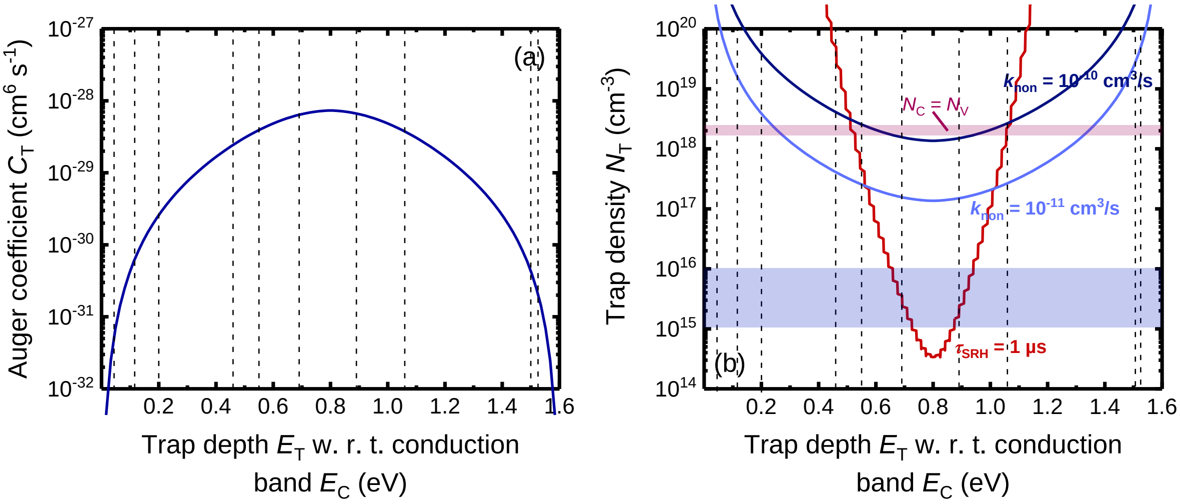

Figure 3: (a) Coefficient C_T of trap-assisted Auger recombination as a function of the trap depth E_T with respect to the conduction band edge E_C. Vertical dashed lines represent trap depths of various intrinsic defects according to Ref. [39]. (b) Trap density N_T as a function of trap depths E_T that would be needed to cause a non-radiative bimolecular recombination coefficient of 10^{-11} and 10^{-10} cm^3/s (light blue and dark blue curves, respectively). In addition, we added the trap density needed to achieve a 1 µs monomolecular lifetime as calculated in ref. [22] based on the theory of multiphonon Shockley-Read-Hall recombination.

TOC Figure

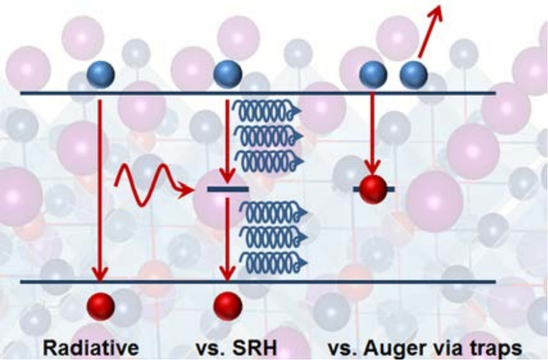

References

(1) Correa-Baena, J. P.; Saliba, M.; Buonassisi, T.; Grätzel, M.; Abate, A.; Tress, W.; Hagfeldt, A. Promises and Challenges of Perovskite Solar Cells. *Science* **2017,** *358*, 739.

(2) Tress, W. Perovskite Solar Cells on the Way to Their Radiative Efficiency Limit – Insights Into a Success Story of High Open-Circuit Voltage and Low Recombination. *Adv. Energy Mater.* **2017,** *7*, 1602358.

(3) Ahrenkiel, R. K. Minority-Carrier Lifetime in III-V Semiconductors. *Minority Carriers in Iii-V Semiconductors: Physics and Applications* **1993,** *39*, 39-150.

(4) Sinton, R. A.; Cuevas, A. Contactless Determination of Current-Voltage Characteristics and Minority-Carrier Lifetimes in Semiconductors From Quasi-Steady-State Photoconductance Data. *Appl. Phys. Lett.* **1996,** *69*, 2510-2512.

(5) Credgington, D.; Durrant, J. R. Insights From Transient Optoelectronic Analyses on the Open-Circuit Voltage of Organic Solar Cells. *J. Phys. Chem. Lett.* **2012,** *3*, 1465-1478.

(6) Abdi-Jalebi, M.; Andaji-Garmaroudi, Z.; Cacovich, S.; Stavrakas, C.; Philippe, B.; Richter, J. M.; Alsari, M.; Booker, E. P.; Hutter, E. M.; Pearson, A. J. et al. Maximizing and Stabilizing Luminescence From Halide Perovskites With Potassium Passivation. *Nature* **2018,** *555*, 497.

(7) Braly, I. L.; deQuilettes, D. W.; Pazos-Outon, L. M.; Burke, S.; Ziffer, M. E.; Ginger, D. S.; Hillhouse, H. W. Hybrid Perovskite Films Approaching the Radiative Limit With Over 90% Photoluminescence Quantum Efficiency. *Nat. Photon.* **2018,** *12*, 355-361.

(8) Ross, R. T. Some Thermodynamics of Photochemical Systems. *J. Chem. Phys.* **1967,** *46*, 4590-4593.

(9) Smestad, G.; Ries, H. Luminescence and Current Voltage Characteristics of Solar-Cells and Optoelectronic Devices. *Sol. Energy Mater. Sol. Cells* **1992,** *25*, 51-71.

(10) Rau, U. Reciprocity Relation Between Photovoltaic Quantum Efficiency and Electroluminescent Emission of Solar Cells. *Phys. Rev. B* **2007,** *76*, 085303.

(11) Steiner, M. A.; Geisz, J. F.; Garcia, I.; Friedman, D. J.; Duda, A.; Olavarria, W. J.; Young, M.; Kuciauskas, D.; Kurtz, S. R. Effects of Internal Luminescence and Internal Optics on V_{oc} and J_{sc} of III-V Solar Cells. *IEEE J. Photov.* **2013,** *3*, 1437-1442.

(12) Miller, O. D.; Yablonovitch, E.; Kurtz, S. R. Strong Internal and External Luminescence As Solar Cells Approach the Shockley-Queisser Limit. *IEEE J. Photov.* **2012,** *2*, 303-311.

(13) Tiedje, T.; Yablonovitch, E.; Cody, G. D.; Brooks, B. G. Limiting Efficiency of Silicon Solar-Cells. *IEEE Trans. Elec. Dev.* **1984,** *31*, 711-716.

(14) Shockley, W.; Read, W. T. Statistics of the Recombination of Holes and Electrons. *Phys. Rev.* **1952,** *87*, 835-842.

(15) Hall, R. N. Electron-Hole Recombination in Germanium. *Phys. Rev.* **1952,** *87*, 387.

(16) Markvart, T. Multiphonon recombination. In *Recombination in Semiconductors*, Landsberg, P. T., Ed.; Cambridge University Press: Cambridge, 2003; p 470.

(17) Markvart, T. Semiclassical Theory of Non-Radiative Transitions. *Journal of Physics C: Solid State Physics* **1981,** *14*, L895.

(18) Ridley, B. K. On the Multiphonon Capture Rate in Semiconductors. *Solid State Electron* **1978,** *21*, 1319-1323.

(19) Ridley, B. K. Multiphonon, Non-Radiative Transition Rate for Electrons in Semiconductors and Insulators. *Journal of Physics C: Solid State Physics* **1978,** *11*, 2323.

(20) Henry, C. H.; Lang, D. V. Nonradiative Capture and Recombination by Multiphonon Emission in GaAs and GaP. *Phys. Rev. B* **1977,** *15*, 989-1016.

(21) Kirchartz, T.; Rau, U. What Makes a Good Solar Cell? *Adv. Energy Mater.* **2018,** *0*, 1703385.

(22) Kirchartz, T.; Markvart, T.; Rau, U.; Egger, D. A. Impact of Small Phonon Energies on the Charge-Carrier Lifetimes in Metal-Halide Perovskites. *The Journal of Physical Chemistry Letters* **2018,** *9*, 939-946.

(23) Benduhn, J.; Tvingstedt, K.; Piersimoni, F.; Ullbrich, S.; Fan, Y.; Tropiano, M.; McGarry, K. A.; Zeika, O.; Riede, M. K.; Douglas, C. J. et al. Intrinsic Non-Radiative Voltage Losses in Fullerene-Based Organic Solar Cells. *Nat. Energy* **2017,** *2*, 17053.

(24) Sendner, M.; Nayak, P. K.; Egger, D. A.; Beck, S.; Muller, C.; Epding, B.; Kowalsky, W.; Kronik, L.; Snaith, H. J.; Pucci, A. et al. Optical Phonons in Methylammonium Lead Halide Perovskites and Implications for Charge Transport. *Mater. Horiz.* **2016,** *3*, 613-620.

(25) Wright, A. D.; Verdi, C.; Milot, R. L.; Eperon, G. E.; Perez-Osorio, M. A.; Snaith, H. J.; Giustino, F.; Johnston, M. B.; Herz, L. M. Electron–Phonon Coupling in Hybrid Lead Halide Perovskites. *Nat. Commun.* **2016,** *7*, 11755.

(26) Richter, J. M.; Abdi-Jalebi, M.; Sadhanala, A.; Tabachnyk, M.; Rivett, J. P. H.; Pazos-Outon, L. M.; Gödel, K. C.; Price, M.; Deschler, F.; Friend, R. H. Enhancing Photoluminescence Yields in Lead Halide Perovskites by Photon Recycling and Light Out-Coupling. *Nat. Commun.* **2016,** *7*, 13941.

(27) Staub, F.; Kirchartz, T.; Bittkau, K.; Rau, U. Manipulating the Net Radiative Recombination Rate in Lead Halide Perovskite Films by Modification of Light Outcoupling. *The Journal of Physical Chemistry Letters* **2017,** *8*, 5084-5090.

(28) Richter, A.; Hermle, M.; Glunz, S. W. Reassessment of the Limiting Efficiency for Crystalline Silicon Solar Cells. *IEEE J. Photov.* **2013,** *3*, 1184-1191.

(29) Richter, A.; Glunz, S. W.; Werner, F.; Schmidt, J.; Cuevas, A. Improved Quantitative Description of Auger Recombination in Crystalline Silicon. *Phys. Rev. B* **2012,** *86*, 165202.

(30) Green, M. A. Limits on the Open-Circuit Voltage and Efficiency of Silicon Solar-Cells Imposed by Intrinsic Auger Processes. *IEEE Trans. Elec. Dev.* **1984,** *31*, 671-678.

(31) Dziewior, J.; Schmid, W. Auger Coefficients for Highly Doped and Highly Excited Silicon. *Appl. Phys. Lett.* **1977,** *31*, 346-348.

(32) Pazos-Outon, L. M.; Xiao, T. P.; Yablonovitch, E. Fundamental Efficiency Limit of Lead Iodide Perovskite Solar Cells. *The Journal of Physical Chemistry Letters* **2018,** *9*, 1703-1711.

(33) Landsberg, P. T.; Rhys-Roberts, C.; Lal, P. Auger Recombination and Impact Ionization Involving Traps in Semiconductors. *Proceedings of the Physical Society* **1964,** *84*, 915.

(34) Baumann, A.; Väth, S.; Rieder, P.; Heiber, M. C.; Tvingstedt, K.; Dyakonov, V. Identification of Trap States in Perovskite Solar Cells. *The Journal of Physical Chemistry Letters* **2015,** *6*, 2350-2354.

(35) Yang, W. S.; Park, B. W.; Jung, E. H.; Jeon, N. J.; Kim, Y. C.; Lee, D. U.; Shin, S. S.; Seo, J.; Kim, E. K.; Noh, J. H. et al. Iodide Management in Formamidinium-Lead-Halide-Based Perovskite Layers for Efficient Solar Cells. *Science* **2017,** *356*, 1376.

(36) Bridgman, P. W. Note on the Principle of Detailed Balancing. *Phys. Rev.* **1928,** *31*, 101-102.

(37) Staub, F.; Hempel, H.; Hebig, J. C.; Mock, J.; Paetzold, U. W.; Rau, U.; Unold, T.; Kirchartz, T. Beyond Bulk Lifetimes: Insights into Lead Halide Perovskite Films From Time-Resolved Photoluminescence. *Phys. Rev. Applied* **2016,** *6*, 044017.

(38) Rau, U.; Paetzold, U. W.; Kirchartz, T. Thermodynamics of Light Management in Photovoltaic Devices. *Phys. Rev. B* **2014,** *90*, 035211.

(39) Yin, W. J.; Shi, T.; Yan, Y. Unusual Defect Physics in $CH_3NH_3PbI_3$ Perovskite Solar Cell Absorber. *Appl. Phys. Lett.* **2014,** *104*, 063903.

(40) Otaredian, T. Separate Contactless Measurement of the Bulk Lifetime and the Surface Recombination Velocity by the Harmonic Optical Generation of the Excess Carriers. *Solid State Electron* **1993,** *36*, 153-162.

(41) Kousik, G. S.; Ling, Z. G.; Ajmera, P. K. Nondestructive Technique to Measure Bulk Lifetime and Surface Recombination Velocities at the Two Surfaces by Infrared Absorption Due to Pulsed Optical Excitation. *J. Appl. Phys.* **1992,** *72*, 141-146.

(42) Stranks, S. D.; Eperon, G. E.; Grancini, G.; Menelaou, C.; Alcocer, M. J. P.; Leijtens, T.; Herz, L. M.; Petrozza, A.; Snaith, H. J. Electron-Hole Diffusion Lengths Exceeding 1 Micrometer in an Organometal Trihalide Perovskite Absorber. *Science* **2013,** *342*, 341-344.

(43) Yang, Y.; Yan, Y.; Yang, M.; Choi, S.; Zhu, K.; Luther, J. M.; Beard, M. C. Low Surface Recombination Velocity in Solution-Grown $CH_3NH_3PbBr_3$ Perovskite Single Crystal. *Nat. Commun.* **2015,** *6*, 7961.

(44) Yang, Y.; Yang, M.; Moore, D.; Yan, Y.; Miller, E.; Zhu, K.; Beard, M. Top and Bottom Surfaces Limit Carrier Lifetime in Lead Iodide Perovskite Films. *Nat. Energy* **2017,** *2*, 16207.

(45) Herz, L. M. Charge-Carrier Mobilities in Metal Halide Perovskites: Fundamental Mechanisms and Limits. *ACS Energy Lett.* **2017,** *2*, 1539-1548.

(46) Brenner, T. M.; Egger, D. A.; Rappe, A. M.; Kronik, L.; Hodes, G.; Cahen, D. Are Mobilities in Hybrid Organic-Inorganic Halide Perovskites Actually "High"? *The Journal of Physical Chemistry Letters* **2015,** *6*, 4754-4757.

(47) deQuilettes, D. W.; Zhang, W.; Burlakov, V. M.; Graham, D. J.; Leijtens, T.; Osherov, A.; Bulovic, V.; Snaith, H. J.; Ginger, D. S.; Stranks, S. D. Photo-Induced Halide Redistribution in Organic-Inorganic Perovskite Films. *Nat. Commun* **2016,** *7*, 11683.

(48) deQuilettes, D. W.; Vorpahl, S. M.; Stranks, S. D.; Nagaoka, H.; Eperon, G. E.; Ziffer, M. E.; Snaith, H. J.; Ginger, D. S. Impact of Microstructure on Local Carrier Lifetime in Perovskite Solar Cells. *Science* **2015,** *348*, 683-686.

(49) Miyata, A.; Mitioglu, A.; Plochocka, P.; Portugall, O.; Wang, J. T.-W.; Stranks, S. D.; Snaith, H. J.; Nicholas, R. J. Direct Measurement of the Exciton Binding

Energy and Effective Masses for Charge Carriers in Organic-Inorganic Tri-Halide Perovskites. *Nat. Phys.* **2015,** *11*, 582-587.

(50) Mosconi, E.; Umari, P.; De Angelis, F. Electronic and Optical Properties of MAPbX3 Perovskites (X = I, Br, Cl): a Unified DFT and GW Theoretical Analysis. *Phys. Chem. Chem. Phys.* **2016,** *18*, 27158-27164.

(51) Zhou, Y.; Huang, F.; Cheng, Y. B.; Gray-Weale, A. Photovoltaic Performance and the Energy Landscape of CH3NH3PbI3. *Phys. Chem. Chem. Phys.* **2015,** *17*, 22604-22615.

(52) Zhou, Y.; Long, G. Low Density of Conduction and Valence Band States Contribute to the High Open-Circuit Voltage in Perovskite Solar Cells. *The Journal of Physical Chemistry C* **2017,** *121*, 1455-1462.

(53) Brivio, F.; Butler, K. T.; Walsh, A.; van Schilfgaarde, M. Relativistic Quasiparticle Self-Consistent Electronic Structure of Hybrid Halide Perovskite Photovoltaic Absorbers. *Phys. Rev. B* **2014,** *89*, 155204.

(54) Crothers, T. W.; Milot, R. L.; Patel, J. B.; Parrott, E. S.; Schlipf, J.; Müller-Buschbaum, P.; Johnston, M. B.; Herz, L. M. Photon Reabsorption Masks Intrinsic Bimolecular Charge-Carrier Recombination in $CH_3NH_3PbI_3$ Perovskite. *Nano Lett.* **2017,** *17*, 5782-5789.

(55) Landi, G.; Neitzert, H. C.; Barone, C.; Mauro, C.; Lang, F.; Albrecht, S.; Rech, B.; Pagano, S. Correlation Between Electronic Defect States Distribution and Device Performance of Perovskite Solar Cells. *Adv. Sci.* **2017,** *4*, 1700183.

(56) Heo, S.; Seo, G.; Lee, Y.; Lee, D.; Seol, M.; Lee, J.; Park, J. B.; Kim, K.; Yun, D. J.; Kim, Y. S. et al. Deep Level Trapped Defect Analysis in $CH_3NH_3PbI_3$ Perovskite Solar Cells by Deep Level Transient Spectroscopy. *Energ. Environ. Sci.* **2017,** *10*, 1128-1133.

(57) Levine, I.; Gupta, S.; Brenner, T. M.; Azulay, D.; Millo, O.; Hodes, G.; Cahen, D.; Balberg, I. Mobility–Lifetime Products in $MAPbI_3$ Films. *J. Phys. Chem. Lett.* **2016,** *7*, 5219-5226.

(58) Gordillo, G.; Otalora, C. A.; Reinoso, M. A. Trap Center Study in Hybrid Organic-Inorganic Perovskite Using Thermally Stimulated Current (TSC) Analysis. *J. Appl. Phys.* **2017,** *122*, 075304.

(59) Duan, H. S.; Zhou, H.; Chen, Q.; Sun, P.; Luo, S.; Song, T. B.; Bob, B.; Yang, Y. The Identification and Characterization of Defect States in Hybrid Organic-Inorganic Perovskite Photovoltaics. *Phys. Chem. Chem. Phys.* **2015,** *17*, 112-116.

(60) Heo, J. H.; Song, D. H.; Han, H. J.; Kim, S. Y.; Kim, J. H.; Kim, D.; Shin, H. W.; Ahn, T. K.; Wolf, C.; Lee, T.-W. et al. Planar $CH_3NH_3PbI_3$ Perovskite Solar Cells With Constant 17.2% Average Power Conversion Efficiency Irrespective of the Scan Rate. *Adv. Mater.* **2015,** *27*, 3424-3430.